

## RESEARCH ARTICLE

# Tubulin polyglutamylation is a general traffic-control mechanism in hippocampal neurons

Satish Bodakuntla<sup>1,2</sup>, Anne Schnitzler<sup>3</sup>, Christopher Villablanca<sup>4,5</sup>, Christian Gonzalez-Billault<sup>4,5</sup>, Ivan Bieche<sup>3,6</sup>, Carsten Janke<sup>1,2,\*</sup> and Maria M. Magiera<sup>1,2,\*</sup>

## ABSTRACT

Neurons are highly complex cells that heavily rely on intracellular transport to distribute a range of functionally essential cargoes within the cell. Post-translational modifications of tubulin are emerging as mechanisms for regulating microtubule functions, but their impact on neuronal transport is only marginally understood. Here, we have systematically studied the impact of post-translational polyglutamylation on axonal transport. In cultured hippocampal neurons, deletion of a single deglutamylase, CCP1 (also known as AGTPBP1), is sufficient to induce abnormal accumulation of polyglutamylation, i.e. hyperglutamylation. We next investigated how hyperglutamylation affects axonal transport of a range of functionally different neuronal cargoes: mitochondria, lysosomes, LAMP1 endosomes and BDNF vesicles. Strikingly, we found a reduced motility for all these cargoes, suggesting that polyglutamylation could act as a regulator of cargo transport in neurons. This, together with the recent discovery that hyperglutamylation induces neurodegeneration, makes it likely that perturbed neuronal trafficking could be one of the central molecular causes underlying this novel type of degeneration.

This article has an associated First Person interview with the first author of the paper.

**KEY WORDS:** Axonal transport, Microtubules, Neuronal transport, Polyglutamylation, Tubulin code, Tubulin posttranslational modifications

## INTRODUCTION

Neurons are the basic structural and functional units of the brain. Insights on how they function as individual cells in a complex neuronal network are instrumental for the bottom-up understanding of brain functions. Our brain contains a vast variety of different types of neurons (Zeng and Sanes, 2017). Some of them are very complex, with long axons (Cavanagh, 1984) and dendritic trees that can be highly ramified (DeFelipe, 2013). Establishment and maintenance of these complex cell morphologies, which is fundamental for the normal function of the brain (Bentley and

Banker, 2016), relies to a large extent on the microtubule cytoskeleton (Conde and Cáceres, 2009). In differentiated neurons, one of the key functions of microtubules is intracellular transport (Nirschl et al., 2017), which ensures the delivery of a large variety of functionally different cargoes, such as organelles (mitochondria, lysosomes and endosomes), proteins or mRNAs to specific target sites inside axons or dendrites (Maday et al., 2014). A key question is thus how transport of those different cargoes is temporally and spatially controlled in order to meet the ever-changing requirements of different neuronal compartments, e.g. synapses, which need to be replenished in receptors for their activity (Choquet and Triller, 2013).

There are several examples demonstrating that different cargoes can be independently regulated in neurons. During neuronal differentiation, mitochondria motility has been shown to progressively decrease, while the transport of late (Rab7-positive) endosomes remained unchanged (Zhou et al., 2016). Even more strikingly, axonal transport of brain-derived neurotrophic factor (BDNF) vesicles was increased while mitochondria motility decreased in differentiating neurons (Moutaux et al., 2018). The independent regulation of mitochondria and BDNF vesicle transport has been further confirmed in cultured neurons from a Huntington's disease mouse model, where BDNF-vesicle transport was reduced, while at the same time mitochondria showed enhanced motility and fragmentation (Virlogeux et al., 2018). These examples illustrate that transport of different axonal cargoes can be independently regulated; however, underlying regulatory mechanisms are not fully understood.

An emerging hypothesis proposes that post-translational modifications (PTMs; Janke, 2014) of microtubule tracks act as 'traffic signs', which are recognized by cargo transporters to control their movements, thus guiding them to their final destinations. A first indication that this could indeed be the case was recently described in dendrites, where anterograde and retrograde transport events take place on microtubules of different polarity, labelled by two distinct PTMs: acetylation and tyrosination (Tas et al., 2017). At this point it remains unclear whether the PTMs are mere markers of those two microtubule populations or whether they participate in guiding the cargo transporters.

A PTM that has attracted attention as a potential active regulator of neuronal trafficking is polyglutamylation. This PTM generates branch chains of glutamate residues on both  $\alpha$ - and  $\beta$ -tubulin (Alexander et al., 1991; Eddé et al., 1990; Rüdiger et al., 1992), thus generating a variety of distinct polyglutamylation patterns. These patterns could destine microtubules to unique functions, e.g. to transport specific cargoes. Initial observations had already shown that altered polyglutamylation could control the delivery of synaptic cargoes (Maas et al., 2009), and we and others have recently demonstrated that abnormally increased polyglutamylation leads to defects in axonal transport of mitochondria (Gilmore-Hall et al., 2019; Magiera et al., 2018).

<sup>1</sup>Institut Curie, PSL Research University, CNRS UMR3348, F-91405 Orsay, France.

<sup>2</sup>Université Paris Sud, Université Paris-Saclay, CNRS UMR3348, F-91405 Orsay, France. <sup>3</sup>Institut Curie, PSL Research University, Department of Genetics, F-75005 Paris, France. <sup>4</sup>Center for Geroscience, Brain Health and Metabolism (GERO), Santiago 7800003, Chile. <sup>5</sup>Department of Biology, Faculty of Sciences, University of Chile, Santiago 7800003, Chile. <sup>6</sup>Université Paris Descartes, Sorbonne Paris Cité, F-75005 Paris, France.

\*Authors for correspondence (maria.magiera@curie.fr; carsten.janke@curie.fr)

ORCID: S.B., 0000-0002-0448-7683; A.S., 0000-0002-1241-170X; C.G.-B., 0000-0003-0335-1482; I.B., 0000-0002-2430-5429; C.J., 0000-0001-7053-2000; M.M.M., 0000-0003-4847-3053

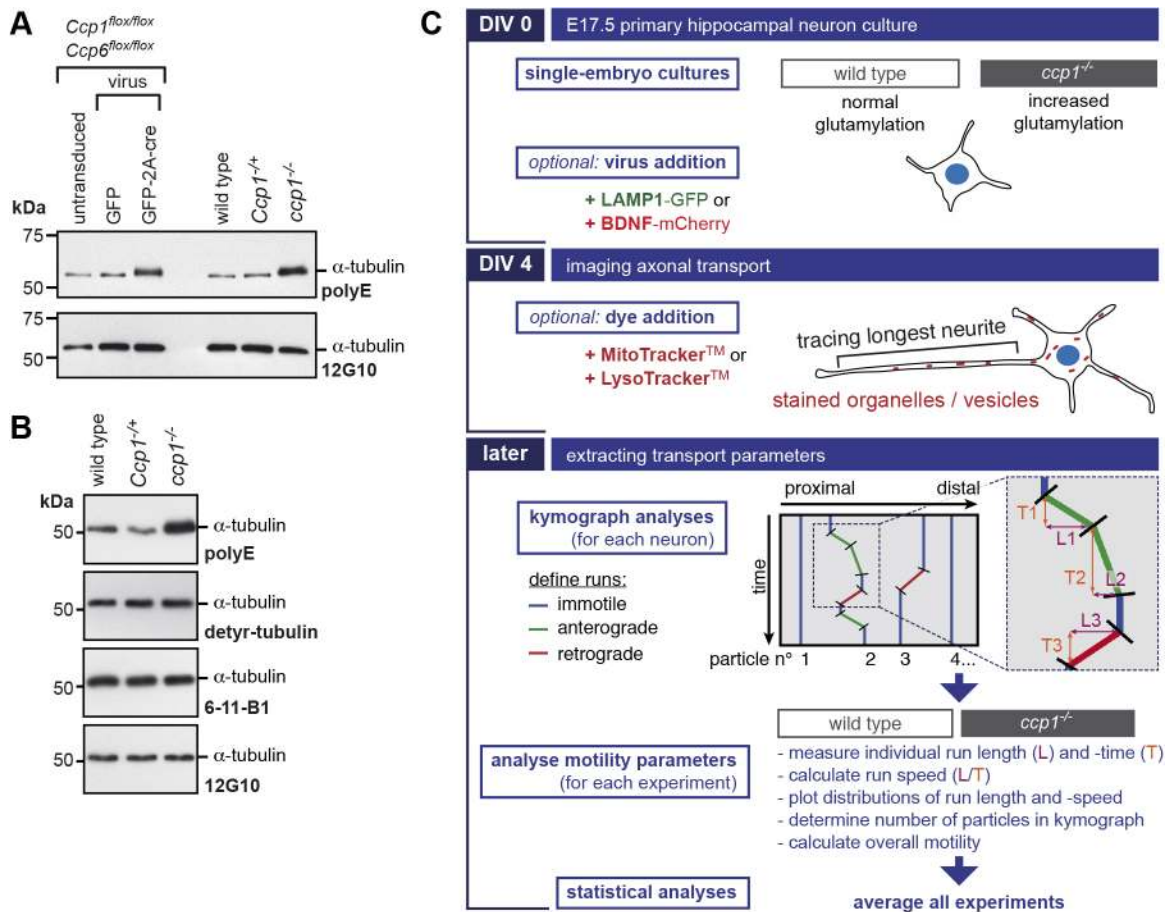


**Fig. 1. Using *Ccp1<sup>-/-</sup>* neurons to determine the impact of tubulin hyperglutamylation in neurons.** (A) Immunoblot of cell extracts of DIV4 *Ccp1<sup>flox/flox</sup>Ccp6<sup>flox/flox</sup>* hippocampal neurons either untransduced, or transduced with lentiviruses encoding GFP or GFP-2A-cre, and hippocampal neurons from wild-type, *Ccp1<sup>+/-</sup>* and *Ccp1<sup>-/-</sup>* embryos probed with an anti-polyglutamylation antibody (polyE).  $\alpha$ -Tubulin levels, detected with the 12G10 antibody, were used as a control for tubulin load. Polyglutamylation levels are increased similarly in neurons transduced with GFP-2A-cre lentivirus and in neurons lacking *Ccp1* (*Ccp1<sup>-/-</sup>*), indicating that removal of *Ccp1* alone is sufficient to induce hyperglutamylation. (B) Hippocampal neurons from wild-type, *Ccp1<sup>+/-</sup>* and *Ccp1<sup>-/-</sup>* embryos probed with anti-polyglutamylation (polyE), anti-detyrosination (detyr-tubulin), anti-acetylation (6-11-B1) and  $\alpha$ -tubulin (12G10) antibodies. Neither detyrosination nor acetylation change in *Ccp1<sup>-/-</sup>* neurons. (C) Experimental flow scheme for the transport experiments shown in Figs 2-5. *Ccp1<sup>-/-</sup>* mice were bred and hippocampi from E17.5 embryos were collected separately for neuronal cultures. In parallel, tissue samples of each embryo were collected and the *Ccp1* genotype determined. Based on the genotyping result, hippocampal neurons from wild-type and *Ccp1<sup>-/-</sup>* embryos were cultured separately. For analysing LAMP1 and BDNF particle transport, lentiviral particles were added to the neurons on DIV0. For analysing mitochondria and lysosomes transport, neurons were treated with MitoTracker and LysoTracker prior to imaging. On DIV4, when the neurons are polarized with a distinct axon, the movements of fluorescently labelled cargoes in at least five wild-type and *Ccp1<sup>-/-</sup>* neurons were recorded for 1 min. Groups of wild-type and *Ccp1<sup>-/-</sup>* neurons that were prepared on the same day were analysed together as one experiment (single experiments are represented in Figs S2, S3, S4 and S5). Differentiated neurons were imaged and the particle movement was analysed by hand-tracing the longest neurite of each recorded neuron, i.e. the axon. A kymograph was generated, and each particle path was fragmented into single runs of constant speed. How single runs were determined is described in detail in the Materials and Methods. We then extracted several parameters such as run length (L) and run time (T), and calculated run speed (L/T), the fraction of time spent in motility and particle density for each cargo type. The results of one complete representative experiment, as well as all kymographs, are shown in the main figures (Figs 2A-F, 3A-F, 4A-F and 5A-F). We next plotted the average of all median values of the independent experiments (Figs S2, S3, S4 and S5) for run speed and run length (Figs 2G,H, 3G,H, 4G,H and 5G,H), as well as the average values of time spent in movement (Figs 2I, 3I, 4I and 5I) and particle densities (Figs 2J, 3J, 4J and 5J).

Until now, however, it has remained unclear whether polyglutamylation is a general trafficking regulator in neurons, or whether this PTM instead controls only selected cargoes. Moreover, polyglutamylation levels and patterns are controlled by a variety of enzymes. Polyglutamylases, which are members of the tubulin tyrosine ligase-like (TLL) family (Janke et al., 2005; van Dijk et al., 2007), and deglutamylases, which belong to the cytosolic carboxypeptidase (CCP) family (Rogowski et al., 2010; Tort et al., 2014), show different enzymatic characteristics and are differentially expressed in different cell types (Ikegami et al., 2006; Kalinina et al., 2007). Their selective expression and/or activation in cells could thus contribute to the generation of characteristic polyglutamylation patterns on microtubule tracks,

which in turn could provide specific signatures that are recognized by only a restricted set of readers. Here, we test the impact of two different deglutamylases, CCP1 and CCP6 (also known as AGTPBP1 and AGLB4, respectively), on polyglutamylation levels in cultured hippocampal neurons, and how excessive polyglutamylation, or hyperglutamylation, affects axonal trafficking of functionally diverse cargoes.

## RESULTS

### Loss of *Ccp1* alone is sufficient to induce tubulin hyperglutamylation in cultured hippocampal neurons

We have previously shown that lack of the deglutamylase *Ccp1* leads to massive and lasting accumulation of hyperglutamylated

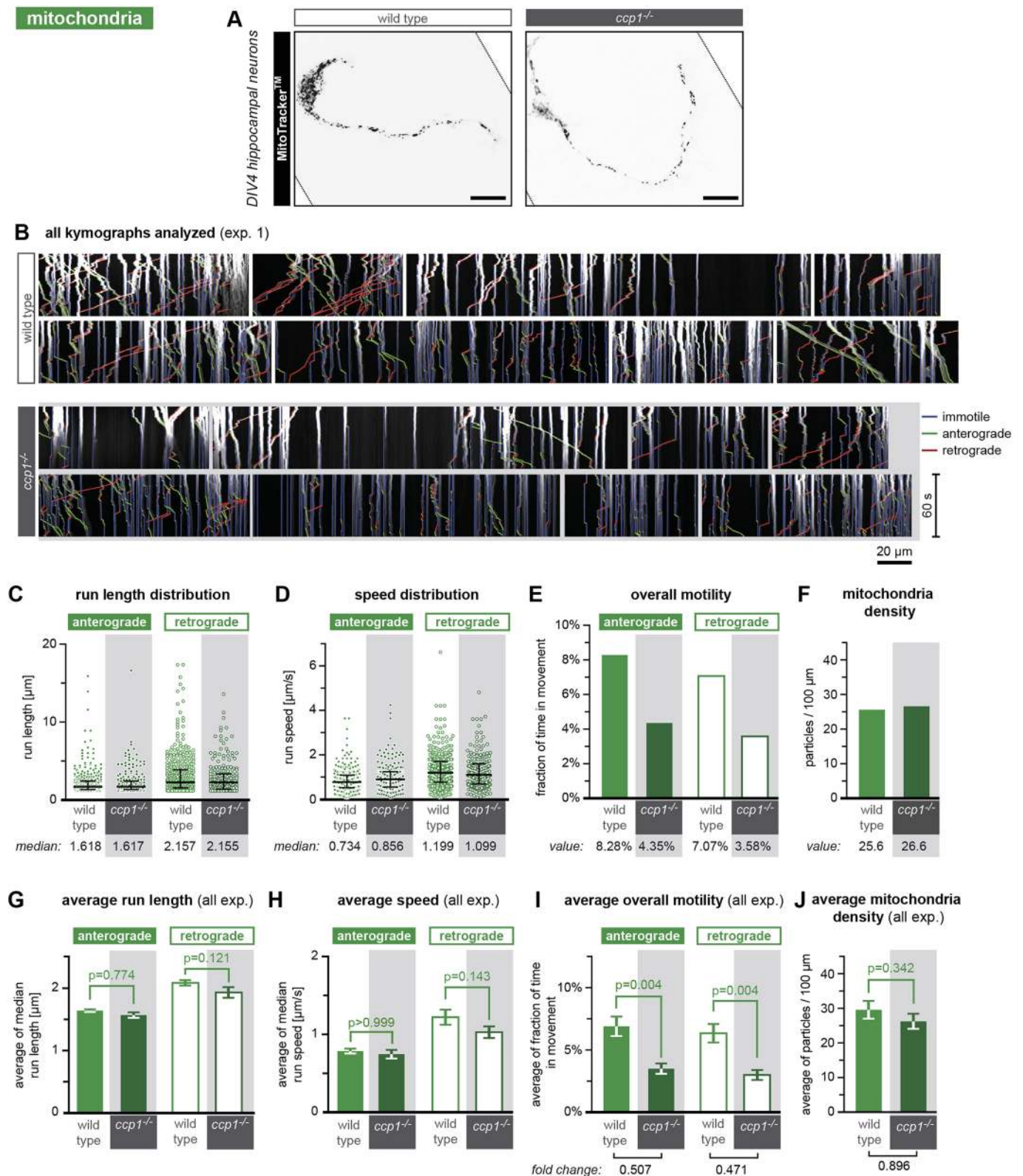


Fig. 2. See next page for legend.

tubulin in the cerebellum and the olfactory bulb. In contrast, other brain regions, such as the cerebral cortex and hippocampus, showed nearly normal levels of polyglutamylation in adult *Ccp1*<sup>-/-</sup> mice (Magiera et al., 2018; Rogowski et al., 2010). Removal of a second deglutamylyase, CCP6, resulted in a strong hyperglutamylation of

all brain regions, including cerebral cortex and hippocampus, indicating that these two enzymes play complementary roles in controlling polyglutamylation patterns in those brain regions. *Ccp1*<sup>-/-</sup>*Ccp6*<sup>-/-</sup> mice showed neurodegeneration of pyramidal neurons in the cerebral cortex, which was observed in neither



**Fig. 2. Increased tubulin polyglutamylation in *Ccp1*<sup>-/-</sup> neurons reduces the overall motility of mitochondria.** Analysis of mitochondria movements in wild-type versus *Ccp1*<sup>-/-</sup> neurons. At DIV4, mitochondria stained with MitoTracker were imaged in the longest extension (axon) of the neuron. Mitochondria movements were recorded for 1 min using a spinning-disk microscope. (A) Representative images (inverted grey scale) of one neuron per genotype stained with MitoTracker (Movie 1, upper panels). Scale bars: 20  $\mu$ m. (B) Kymographs of mitochondria movements for all neurons analysed within one single experiment (exp. 1; corresponding kymostacks are shown in Movie 1, lower panels). Each run is defined as a continuous movement of the mitochondria without a change in direction or speed. Anterograde and retrograde runs are colour-coded in green and red, respectively, while immotile events are shown in blue. Scale bars: 60 s; 20  $\mu$ m. (C-F) Analyses of one single experiment (exp. 1; B) for (C) run length and (D) run speed of mitochondria shown as scatter plots where each point represents the value of a single run. The horizontal black line indicates the median of the distribution with whiskers at the interquartile range. Numerical values of the medians are indicated below each respective distribution. Light-green circles are for wild type and dark-green circles on a grey background are for *Ccp1*<sup>-/-</sup>. Filled circles are for anterograde and open circles are for retrograde direction. (E) Fraction of time spent in motility (overall motility) and (F) mitochondrial density from this experiment are represented as bar graphs. (G-J) Statistical analyses of four independent experiments (each of them shown separately in Fig. S2): average (G) run length, (H) run speed, (I) overall motility and (J) mitochondrial density are shown as mean  $\pm$  s.e.m. Filled bars show anterograde movements; open bars retrograde movements. Light-green bars are for wild-type and dark-green bars on a grey background are for *Ccp1*<sup>-/-</sup> neurons.

*Ccp1*<sup>-/-</sup> nor *Ccp6*<sup>-/-</sup> mice, and thus is likely to be a direct result of hyperglutamylation (Magiera et al., 2018).

To investigate the cellular mechanisms affected by the absence of these two deglutamylases, we used cultured primary hippocampal neurons (Kaech and Banker, 2006) in which the knockout of both *Ccp1* and *Ccp6* was induced by cre-mediated recombination, leading to a massive increase in polyglutamylation in these neurons (Bodakuntla et al., 2020a). At the same time, however, we had observed that polyglutamylation is also increased in hippocampi of young *Ccp1*<sup>-/-</sup> mice, but, in contrast to *Ccp1*<sup>-/-</sup>*Ccp6*<sup>-/-</sup> mice, did not persist into adulthood (Magiera et al., 2018). As this suggested that loss of *Ccp1* alone might be sufficient to induce tubulin hyperglutamylation in young hippocampal neurons, we directly compared induced *Ccp1*<sup>-/-</sup>*Ccp6*<sup>-/-</sup> with *Ccp1*<sup>-/-</sup> neurons. As previously shown (Bodakuntla et al., 2020a; Magiera et al., 2018), expression of cre-recombinase in *Ccp1*<sup>flox/flox</sup>*Ccp6*<sup>flox/flox</sup> neurons resulted in hyperglutamylation of tubulin. Strikingly, a direct comparison on the same immunoblot showed that *Ccp1*<sup>-/-</sup> neurons have a similar, or even slightly higher level of hyperglutamylation when compared with induced *Ccp1*<sup>-/-</sup>*Ccp6*<sup>-/-</sup> neurons at DIV4 (4 days *in vitro*; Fig. 1A). Two tubulin PTMs that had previously been linked to axonal transport, acetylation (Dompiere et al., 2007; Kim et al., 2016) and detyrosination (Konishi and Setou, 2009) were not altered in *Ccp1*<sup>-/-</sup> neurons (Fig. 1B). These results indicate that loss of *Ccp1* alone is sufficient to induce hyperglutamylation in young hippocampal neurons, which could be explained by the relatively low expression of *Ccp6* in cultured hippocampal neurons when compared with adult hippocampus (Fig. S1). We thus aimed at testing whether this *Ccp1*<sup>-/-</sup>-induced hyperglutamylation is functionally equivalent to the hyperglutamylation generated by the loss of *Ccp1* and *Ccp6* in its ability to affect axonal transport.

#### Loss of CCP1 is sufficient to reduce mitochondria transport

To determine whether the previously observed reduction of mitochondria motility in *Ccp1*<sup>-/-</sup>*Ccp6*<sup>-/-</sup> neurons (Magiera et al., 2018) could be fully reproduced by removing *Ccp1* alone, we crossed *Ccp1*<sup>-/+</sup> mice, from which we prepared single-embryo

primary neuron cultures. This allowed us to obtain both, *Ccp1*<sup>-/-</sup> (hyperglutamylated) and wild-type (control) neurons side by-side, and measure axonal transport in parallel.

We analysed the movements of mitochondria labelled with the fluorescent dye MitoTracker (Fig. 2; Fig. S2) as performed previously for *Ccp1*<sup>-/-</sup>*Ccp6*<sup>-/-</sup> neurons (Magiera et al., 2018). First, we verified that mitochondria densities did not differ between wild-type and *Ccp1*<sup>-/-</sup> neurons (Fig. S2D). Next, we assigned runs, defined as trajectories during which particles move without interruption at constant speed (Fig. 1C; Bodakuntla et al., 2020b). Run length and run speed were quantified and plotted separately for each experiment to determine medians (Fig. S2A,B). The overall time the entire particle pool spent in movement (overall motility) was determined as the sum of all run durations relative to the overall number of particles in the field (Fig. S2C).

Almost identical to previous measurements in *Ccp1*<sup>-/-</sup>*Ccp6*<sup>-/-</sup> neurons (Magiera et al., 2018), tubulin hyperglutamylation generated by loss of *Ccp1* alone (*Ccp1*<sup>-/-</sup>) reduced the fraction of time mitochondria spent in movement by about 50% (Fig. 2I) in both anterograde and retrograde directions, without affecting run length or run speed (Fig. 2G,H). These results confirm that hyperglutamylation induced by loss of *Ccp1* alone has the same impact on axonal transport of mitochondria as the double-knockout of *Ccp1* and *Ccp6* (Magiera et al., 2018), and validates *Ccp1*<sup>-/-</sup> neurons as model system for testing the effect of hyperglutamylation on the transport of other axonal cargoes.

#### Hyperglutamylation downregulates motility of lysosomal/endosomal particles

We next aimed at determining the impact of *Ccp1*<sup>-/-</sup>-induced hyperglutamylation on the motility of lysosomes, endosomes and autophagosomes. For this, we used two complementary labelling approaches: the fluorescent dye LysoTracker (Fig. 3; Fig. S3) to label lysosomes but also autophagosomes (Maday et al., 2012), and expression of the lysosome-associated membrane protein 1 (LAMP1)-GFP (Fig. 4; Fig. S4) to label non-degradative lysosomal, as well as endocytic vesicles. Both markers label partially overlapping, but not identical vesicle fractions (Cheng et al., 2018). LysoTracker was added to the neurons prior to the transport analyses at DIV4, while LAMP1-GFP was transduced into the cultured neurons at DIV0 using lentiviral vectors (Fig. 1C), resulting in a strong vesicle labelling at DIV4.

We analysed these two markers using the paradigm established for mitochondria (Figs 1C and 2). Run length and run speed in both anterograde and retrograde directions were unchanged by hyperglutamylation (*Ccp1*<sup>-/-</sup>; Figs 3G,H and 4G,H). The time spent in movement decreased for both LysoTracker-positive (Fig. 3I) and LAMP1-GFP vesicles (Fig. 4I), however to different extents. LAMP1-GFP vesicles showed about 30% less motility in both anterograde and retrograde directions (Fig. 4I), whereas anterograde movements of LysoTracker-labelled vesicles were reduced by only about 15% (Fig. 3I).

These observations consistently demonstrate that hyperglutamylation impedes the motility of both vesicle populations. The lower impact on the anterograde motility of LysoTracker-positive particles might be explained by the low number of anterograde runs observed for this marker (Lee et al., 2011). In contrast, LAMP1, which in the past has been routinely used as a lysosomal marker (Ashrafi et al., 2014; Lee et al., 2011), was recently shown to label both non-degradative lysosomal and endocytic vesicles (Cheng et al., 2018), which explains the higher number of anterograde transport events (Klinman and Holzbaur, 2016).

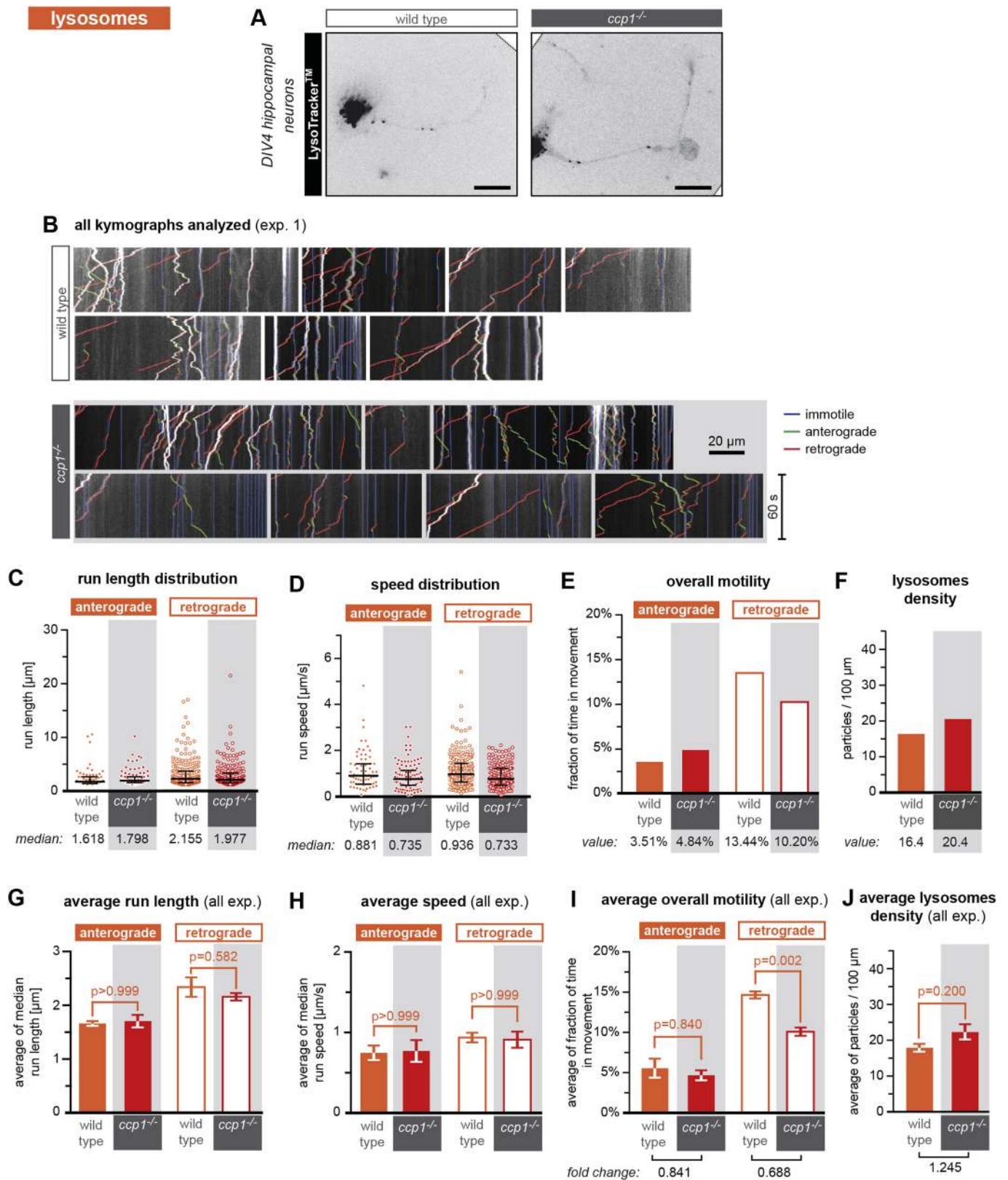


Fig. 3. See next page for legend.

### Regulation of axonal transport by polyglutamylation is not restricted to kinesin 1-driven cargoes

The anterograde transport of mitochondria, lysosomes and LAMP1-positive endosomes is predominantly driven by motors of the

kinesin 1 (KIF5) family. To test whether polyglutamylation also impacts transport of cargoes that use different motor proteins, we analysed BDNF vesicles that are transported by a kinesin 3 motor protein, KIF1A (Lo et al., 2011).

**Fig. 3. Increased tubulin polyglutamylation reduces the overall motility of lysosomes.** Analysis of lysosome movements in wild-type versus *Ccp1*<sup>-/-</sup> neurons. At DIV4, lysosome movements labelled with LysoTracker were imaged in the axon for 1 min using a spinning-disk microscope.

(A) Representative images (inverted grey scale) of one neuron per genotype stained with LysoTracker (Movie 2, upper panels). Scale bars: 20  $\mu$ m. (B) Kymographs of lysosome movements for all neurons analysed within one single experiment (exp. 1; all corresponding kymostacks are shown in Movie 2, lower panels). Scale bars: 60 s; 20  $\mu$ m. (C-F) Analyses of one single experiment (exp. 1; B) for (C) run length and (D) run speed of lysosomes shown as scatter plots as shown in Fig. 2, where each point represents the value of a single run. Light-orange circles are for wild type and dark-orange circles on a grey background are for *Ccp1*<sup>-/-</sup>. Filled circles are for anterograde direction; open circles are for retrograde direction. (E) Fraction of time spent in motility (overall motility) and (F) lysosome density from this experiment are represented as bar graphs. (G-J) Statistical analyses of four independent experiments (each of them shown separately in Fig. S3): average (G) run length, (H) run speed, (I) overall motility and (J) lysosome density are shown as mean  $\pm$  s.e.m. Filled bars show anterograde movements; open bars show retrograde movements. Light-orange bars are for wild-type and dark-orange bars on a grey background are for *Ccp1*<sup>-/-</sup> neurons.

BDNF vesicles were visualized by virus-mediated expression of BDNF-mCherry (Fig. 5; Fig. S5). As for all other cargoes measured so far, we found that BDNF-mCherry-positive vesicles do not alter run length and run speed in either anterograde or retrograde directions under hyperglutamylation (*Ccp1*<sup>-/-</sup>) conditions (Fig. 5G,H). However, the time spent in movement was reduced by about 50% in anterograde, and about 40% in retrograde direction (Fig. 5I). This strongly suggests that the reduction of the anterograde trafficking we had measured for mitochondria (Fig. 2I) and LAMP1-positive endosomes (Fig. 4I) is not a specific feature of kinesin 1 motors, but appears to be a more general mechanism that is effective for a range of transport cargoes driven by different motor proteins.

### Polyglutamylation specifically affects long runs of BDNF vesicles

As mentioned before, all transport cargoes analysed showed similar median run lengths between wild-type and *Ccp1*<sup>-/-</sup> neurons (Figs S2A; S3A; S4A and S5A). However, we noticed that specifically for BDNF vesicles, the highest values, which constitute only a small share of the entire pool of runs, appeared reduced in *Ccp1*<sup>-/-</sup> neurons. To test this possibility, we performed a bin analysis for the run length measurements for each cargo. As we were interested in determining the probability of long runs, the bin width was chosen about twice the median values (3  $\mu$ m for anterograde runs of mitochondria and lysosomes; 6  $\mu$ m for anterograde runs of LAMP1-GFP and BDNF-mCherry vesicles; 5  $\mu$ m for all retrograde runs; Fig. 6).

Owing to strong variations in the proportion of long runs between individual experiments, statistical analyses did not show significant differences, which is why we compared corresponding values for wild-type and *Ccp1*<sup>-/-</sup> neurons for each experimental set (Fig. 6). Strikingly, while mitochondria, lysosomes and LAMP1-positive endosomes showed random patterns in these analyses (Fig. 6A-C), we observed a persistent trend for a decrease in the percentage of long runs for BDNF vesicles in neurons with tubulin hyperglutamylation (*Ccp1*<sup>-/-</sup>) in both anterograde and retrograde directions (Fig. 6D). This unique trend could be related to the transport of BDNF vesicles by KIF1A (Lo et al., 2011), in contrast to KIF5 for the other cargoes.

Indeed, a recent *in vitro* study comparing KIF1A motility on microtubules assembled from HeLa cell and brain tubulin found a

reduced overall run length (defined as the sum of continuous run lengths during a single motility event on the microtubule) of KIF1A on brain microtubules (Lessard et al., 2019), which, in contrast to HeLa cell microtubules, are polyglutamylation. However, as HeLa cell tubulin differs from brain tubulin in several PTMs (Barisic et al., 2015) and tubulin isotypes (Newton et al., 2002); conclusive evidence that our observation is directly related to an altered behaviour of KIF1A on hyperglutamylation microtubules is still elusive. Similarly, the increased percentage of long runs in the retrograde direction cannot be explained by the motor protein dynein, which drives retrograde transport of all vesicles we analysed. However, dynein can associate with a variety of adaptor proteins (Reck-Peterson et al., 2018), which might affect the overall transport behaviour of different cargoes in a polyglutamylation-dependent manner.

### DISCUSSION

Regulation of axonal transport in neurons is an essential process for neuronal function and homeostasis (Guedes-Dias and Holzbaur, 2019), in which many different cargoes need to be delivered to specific locations in a timely manner. Here, we have analysed the impact of tubulin polyglutamylation on axonal transport of cargoes that are functionally and structurally distinct, and that had been previously shown to be differentially regulated under specific physiological conditions (Moutaux et al., 2018; Virlogeux et al., 2018; Zhou et al., 2016). Mitochondria, the main source of cellular ATP, are constantly shuttled in neurons to be docked locally in regions demanding an energy supply, such as the growth cones (Morris and Hollenbeck, 1993) and presynaptic boutons (Lee and Peng, 2008; Rowland et al., 2000). Lysosomes and late endosomes are degradation hubs for misfolded proteins and malfunctioning organelles, which are predominantly transported to the cell body for complete degradation, a process essential for neuronal survival (Pu et al., 2016). BDNF vesicles deliver this neuropeptide to its target sites – synapses – where it controls synaptic plasticity and maturation (Lu et al., 2013). Aberrations of axonal transport can thus lead to severe perturbations in neuronal function and homeostasis, and consequently play key roles in neurodegeneration (Brady and Morfini, 2017; Millecamps and Julien, 2013; Sleight et al., 2019). Here, we show that post-translational polyglutamylation of neuronal microtubules can regulate the transport of functionally diverse cargoes in hippocampal neurons (Fig. 7A).

### How does microtubule polyglutamylation regulate axonal transport?

Axonal transport is regulated at different levels. It is determined (1) by the type of motor proteins that move the cargo, or by additional proteins that are integral parts of transport vesicles/organelles (Hirokawa et al., 2010). Moreover, (2) cellular MAPs, by binding to the microtubule tracks, can act as ‘road blocks’ for the transport complexes (Vershinin et al., 2007; discussed by Bodakuntla et al., 2019; Tortosa et al., 2016); or (3) changes in the overall architecture and integrity of the microtubule cytoskeleton could impact the delivery of cargoes inside neurons (Yogev et al., 2016). PTMs of the microtubule tracks could provide guidance and specificity to different types of transport cargoes, and, strikingly, could directly perturb all of the above-listed transport-regulating mechanisms in case of hyperglutamylation (Fig. 7B).

Emerging data from *in vitro* studies demonstrate that tubulin polyglutamylation can directly interfere with the attachment and processivity of (1) the motor proteins (Sirajuddin et al., 2014), and



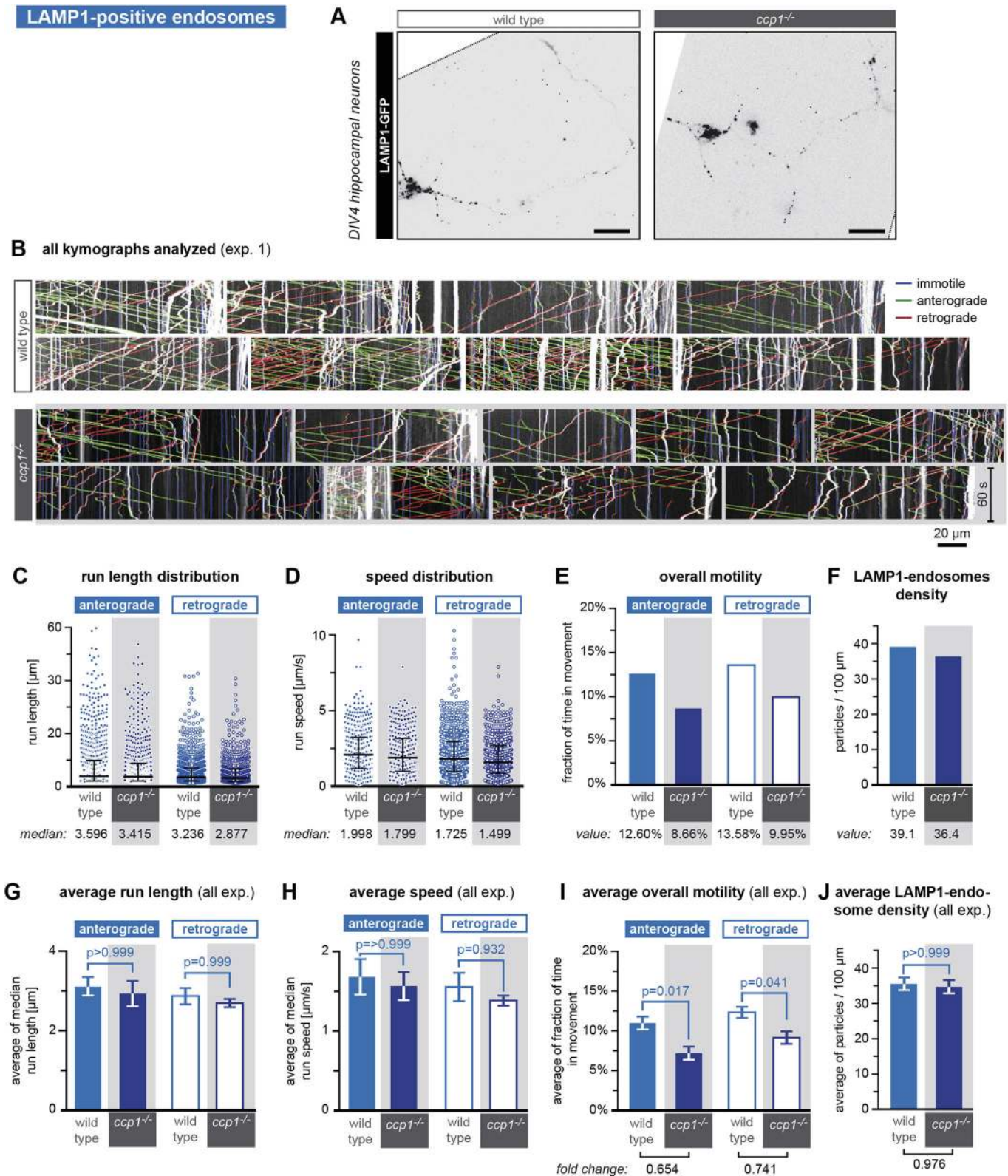


Fig. 4. See next page for legend.

that different motor proteins show different sensitivity to tubulin glutamylation. Kinesin 3, for example, which carries BDNF vesicles, was suggested to be sensitive to polyglutamylation (Lessard et al., 2019), which could at least partially explain the stronger impact of hyperglutamylation on BDNF vesicles when

compared with LAMP1 vesicles or lysosomes, which are both carried by kinesin 1 (Hirokawa et al., 2010). Previous data have also suggested that (2) MAPs could be sensitive to tubulin polyglutamylation, in particular the neuronal MAPs tau, MAP2 and MAP1 (Bonnet et al., 2001; Boucher et al., 1994). The

**Fig. 4. Increased tubulin polyglutamylation reduces the overall motility of LAMP1 endosomes.** Analysis of LAMP1-positive endosome movements in wild-type versus *Ccp1*<sup>-/-</sup> neurons. Neurons were transduced with LAMP1-GFP lentivirus at DIV0, and movements of LAMP1-positive particles were imaged at DIV4 for 1 min using a spinning-disk microscope. (A) Representative images (inverted grey scale) of one neuron per genotype expressing LAMP1-GFP (Movie 3, upper panels). Scale bars: 20  $\mu$ m. (B) Kymographs of LAMP1-endosome movements for all neurons analysed within one single experiment (exp. 1; all corresponding kymostacks are shown in Movie 3, lower panels). Scale bars: 60 s; 20  $\mu$ m. (C-F) Analyses of one single experiment (exp. 1; B) for (C) run length and (D) run speed of LAMP1 endosomes shown as scatter plots as shown in Fig. 2, where each point represents the value of a single run. Light-blue circles are for wild type and dark-blue circles on a grey background are for *Ccp1*<sup>-/-</sup>. Filled circles are for anterograde direction; open circles are for retrograde direction. (E) Fraction of time spent in motility (overall motility) and (F) LAMP1 endosome density from this experiment are shown. (G-J) Statistical analyses of three independent experiments (each of them shown separately in Fig. S4): average (G) run length, (H) run speed, (I) overall motility and (J) LAMP1 endosome density are shown as mean  $\pm$  s.e.m. Filled bars show anterograde movements; open bars show retrograde movements. Light-blue bars are for wild-type and dark-blue bars on a grey background are for *Ccp1*<sup>-/-</sup> neurons.

differential binding and distribution of MAPs could also affect the (3) overall architecture of the microtubule cytoskeleton (Harada et al., 1994). For example, microtubules decorated with neuronal tau or MAP2 show different spacing in neuronal projections (Chen et al., 1992): MAP2, which contains longer projection domains, pushes microtubules further apart and might thus create additional space for the passage of transport cargoes. Microtubule spacing had been indeed shown to control axonal trafficking, with consequences on synaptic functions in *Drosophila* neurons (Stephan et al., 2015). Moreover, a link between microtubule spacing, mitochondria transport and tau protein phosphorylation has been established in murine cortical neurons (Shahpasand et al., 2012). At the same time, changes in polyglutamylation could also alter the architecture of the microtubule cytoskeleton by controlling the activity of microtubule-severing enzymes, such as spastin (Lacroix et al., 2010; Valenstein and Roll-Mecak, 2016), which in turn could affect transport. However, our observation that knocking out spastin in *Ccp1*<sup>-/-</sup> mice did not rescue hyperglutamylation-induced degeneration of Purkinje cells (Magiera et al., 2018) suggested that microtubule severing might not be the key molecular defect induced by upregulation of polyglutamylation.

#### Specificity of transport regulation by polyglutamylation

In hippocampal pyramidal cells used in our study, upregulation of polyglutamylation affected a range of functionally different axonal cargoes, suggesting that polyglutamylation could act as a general traffic-control mechanism. However, axonal transport of the same cargoes can be differentially regulated in different types of neurons (Her and Goldstein, 2008). Indeed, a recent study using cerebellar granule cells lacking CCP1 found no significant reduction for endosomal transport in the granule cells with hyperglutamylation (Gilmore-Hall et al., 2019), while at the same time mitochondria transport was perturbed to a similar degree as in hippocampal neurons. Although a definite explanation for these differences cannot be given, one possibility is that various polyglutamylases are differentially expressed or active in different neuronal types, and consequently generate distinct patterns of hyperglutamylation upon the deletion of deglutamylases. These distinct patterns would in turn affect different transport cargoes, thus leading to neuron-type specific effects of hyperglutamylation.

The conclusion that transport specificity is controlled by the glutamylating rather than by the deglutamylating enzymes is

also supported by our observation that mitochondria transport is similarly reduced in hippocampal neurons lacking CCP1 alone and both CCP1 and CCP6, because in both cases the accumulating polyglutamylation is generated by the same set of polyglutamylases in these neurons. It will thus be important to investigate the impact of single polyglutamylases on the transport of different cargoes.

#### Physiological implications

Notwithstanding the underlying mechanisms, our findings demonstrate that polyglutamylation is a post-translational mechanism that regulates the transport of a range of neuronal cargoes, and could thus play an important role in controlling vital neuronal functions. Polyglutamylation-related changes in neuronal transport had been previously linked to the delivery of synaptic vesicles (Ikegami et al., 2007), and shown to be activity-dependent (Maas et al., 2009), but direct transport measurements had not been performed. Our analyses thus directly validate these initial findings, and underpin the conceptual idea that, by controlling axonal transport (Guedes-Dias and Holzbaur, 2019), polyglutamylation could directly control neuronal activity and eventually memory by controlling synaptic function.

Most importantly, our finding that transport of functionally different cargoes is perturbed in neurons with hyperglutamylation strengthens the hypothesis that degeneration of neurons with mutated *Ccp1* (Gilmore-Hall et al., 2019; Magiera et al., 2018; Shashi et al., 2018) could be linked to a dysfunction of intra-neuronal transport in different types of neurons. Understanding the mechanisms of polyglutamylation in the regulation of neuronal homeostasis becomes increasingly relevant as more and more reports link mutations in deglutamylases to human neurodegenerative disorders (Karakaya et al., 2019; Shashi et al., 2018; Sheffer et al., 2019; Vélez et al., 2016).

#### Conclusions

Together, the results of our analyses highlight the emerging role of tubulin polyglutamylation as a key regulator of neuronal transport, and its perturbation as a causative factor for neurodegenerative disorders. An intriguing issue to be addressed in the future is how polyglutamylation relates to other tubulin PTMs that are also present in neurons, such as detyrosination and acetylation, both of which are known to also affect transport (Dompierre et al., 2007; Kim et al., 2016; Konishi and Setou, 2009). Our gene expression analyses (Fig. S1) show that enzymes involved in tubulin detyrosination and acetylation are at their highest expression levels in the young, undifferentiated neurons. In contrast, enzymes involved in polyglutamylation show an increasing expression throughout development, and persistent expression into adulthood. This strongly suggests that polyglutamylation, by remaining particularly dynamic in adult neurons, plays a central role in adapting cargo transport to physiological requirements and activity of neurons throughout life, thus assuring neuronal homeostasis.

#### MATERIALS AND METHODS

##### Mouse lines

All the animals in this study were used in accordance with the recommendations of the European Community (2010/63/UE). Experimental procedures were specifically approved by the ethics committee of the Institut Curie CEEA-IC #118 (authorization number 04395.03 given by the National Authority) in compliance with the international guidelines.

Generation of *Ccp1*<sup>-/-</sup> and *Ccp1*<sup>lox/lox</sup>*Ccp6*<sup>lox/lox</sup> mice has been described in detail before (Magiera et al., 2018; Muñoz-Castañeda et al., 2018). All embryos and mice, both male and female, were used in this study.



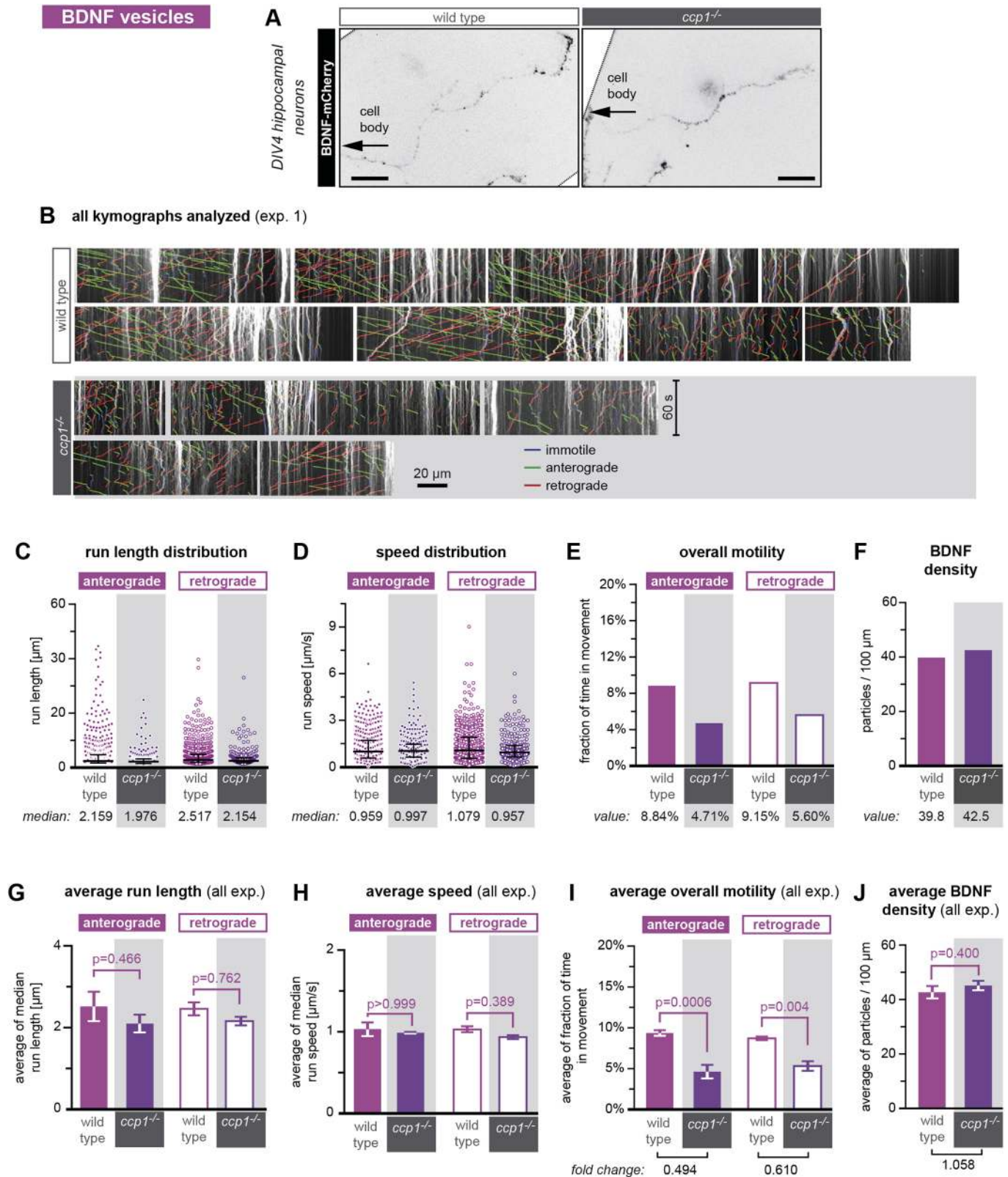


Fig. 5. See next page for legend.

### Genotyping

For adult mice, DNA was extracted from ear fragments (collected during the identification of mice) or tail fragments by proteinase K digestion. Lysis buffer [0.1 M Tris-HCl (pH 8) (Sigma, T1503), 0.2 M NaCl (Sigma, S3014), 5 mM EDTA (Euromedex, EU0007-C) and 0.4% SDS

(Euromedex, EU0660)] containing 0.1 mg/ml proteinase K (193504, MP Biomedicals) was added to the sample, incubated at 56°C for 4 h and for 10 min at 95°C. For hippocampal neuron cultures, a piece of the brain tissue from the E17.5 embryos was lysed using REDextract-N-Amp Tissue PCR Kit (Sigma, XNAT) using the manufacturer's instructions. PCR-based

**Fig. 5. Increased tubulin polyglutamylation reduces the overall motility of BDNF vesicles.** Analysis of BDNF vesicle movements in wild-type versus *Ccp1*<sup>-/-</sup> neurons. Neurons were transduced with BDNF-mCherry lentivirus at DIV0, and movements of BDNF-positive particles were imaged at DIV4 for 1 min using a spinning-disk microscope. (A) Representative images (inverted grey scale) of one neuron per genotype expressing BDNF-mCherry (Movie 4, upper panels). Scale bars: 20  $\mu$ m. (B) Kymographs of BDNF-vesicle movements for all neurons analysed within one single experiment (exp. 1; all corresponding kymostacks are shown in Movie 4, lower panels). Scale bars: 60 s; 20  $\mu$ m. (C-F) Analyses of one single experiment (exp. 1; B) for (C) run length and (D) run speed of BDNF vesicles shown as scatter plots as in Fig. 2, where each point represents the value of a single run. Light-purple circles are for wild type and dark-purple circles on a grey background are for *Ccp1*<sup>-/-</sup>. Filled circles are for anterograde direction; open circles are for retrograde direction. (E) Fraction of time spent in motility (overall motility) and (F) BDNF-vesicle density from this experiment are shown. (G-J) Statistical analyses of three independent experiments (each of them shown separately in Fig. S5): average (G) run length, (H) run speed, (I) overall motility and (J) BDNF-vesicle density are shown as mean  $\pm$  s.e.m. Filled bars show anterograde movements; open bars show retrograde movements. Light-purple bars are for wild-type and dark-purple bars on a grey background are for *Ccp1*<sup>-/-</sup> neurons.

genotyping was carried out using the primers and protocols described in our earlier studies (Bodakuntla et al., 2020a; Magiera et al., 2018).

### RNA isolation and RT-qPCR

Total RNA from mouse hippocampal neurons cultured for 1, 4, 7 or 10 days, as well as entire hippocampi from mice of different ages was isolated using the Trizol reagent (Life Technologies) following the manufacturer's instructions. Concentrations and quality of the extracted RNA was determined with a Nanodrop Spectrophotometer (Thermo Fisher Scientific). cDNA for these RNAs was synthesized using the SYBRGreen

Master Mix kit. PCR amplification was performed on an ABI Prism 7900 Sequence Detection System (Perkin-Elmer Applied Biosystems) as described in detail elsewhere (Bièche et al., 1999). Reverse transcription real-time quantitative PCR (RT-qPCR) was performed for all the known tubulin-modifying enzymes,  $\beta$ 3-tubulin (TUBB3) and for the TATA-binding protein (*Tbp*) gene (NM\_013684), which was used as a control. PCR conditions are available upon request. The relative mRNA expression levels were represented as the N-fold difference in target gene expression relative to the *Tbp* gene (termed ' $N_{\text{target}}$ ') and calculated as  $N_{\text{target}} = 2^{\Delta\Delta\text{Ct}_{\text{sample}}}$ . The value of the cycle threshold ( $\Delta\text{Ct}$ ) of a given sample was determined by subtracting the average Ct value of the target gene from the average Ct value for the *Tbp* gene. Primers used in this study are shown in Table S1.

### Sample preparation and immunoblotting

Hippocampal neurons transduced on DIV4 (4 days *in vitro*). Wild type, *Ccp1*<sup>-/+</sup>, *Ccp1*<sup>-/-</sup> or *Ccp1*<sup>fllox/fllox</sup>*Ccp6*<sup>fllox/fllox</sup> transduced with lentivirus encoding GFP or GFP-2A-cre were collected in 2 $\times$  Laemmli buffer [180 mM DTT (Sigma, D9779), 4% SDS (VWR #442444H), 160 mM Tris-HCl (pH 6.8), 20% glycerol (VWR #24388.295) and bromophenol blue]. The samples were then boiled at 95°C for 5 min, spun down at 20,000 g for 5 min using a table top centrifuge and stored at -20°C. Samples were loaded on SDS-PAGE gels, separated and transferred onto a nitrocellulose membrane using Bio-Rad Trans-Blot Turbo system, according to the manufacturer's instructions. The membranes were incubated with an anti- $\alpha$ -tubulin antibody [12G10, 1:1000 (vol/vol); developed by J. Frankel and M. Nelson, obtained from the Developmental Studies Hybridoma Bank, developed under the auspices of the NICHD, and maintained by the University of Iowa], an anti-acetylated K40 tubulin [6-11B-1, 1:2000 (vol/vol); Sigma T6793], an anti-detyrosinated tubulin [1:1000 (vol/vol); Millipore AB3201] and an anti-polyglutamylated tubulin antibody

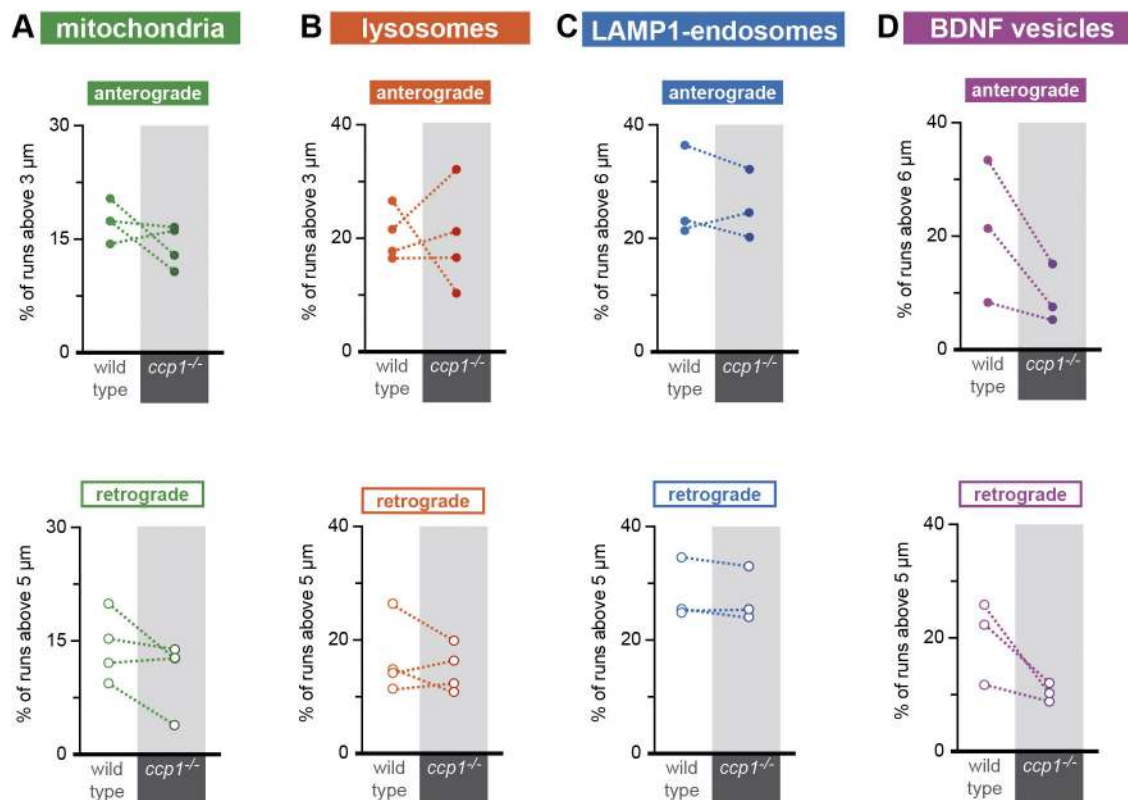


**Fig. 6. Tubulin hyperglutamylation affects long runs of BDNF vesicles.** (A-D) Bin analyses of anterograde and retrograde run lengths of (A) mitochondria, (B) lysosomes, (C), LAMP1-GFP endosomes and (D) BDNF-mCherry vesicles were performed to determine the probability of long runs in wild-type versus *Ccp1*<sup>-/-</sup> neurons. The bin values, defined as twice the median value of the run length distributions were: 3  $\mu$ m for anterograde runs of mitochondria and lysosomes; 6  $\mu$ m for anterograde runs of LAMP1-GFP and BDNF-mCherry vesicles; and 5  $\mu$ m for all retrograde runs. Pairs of connected points represent values from wild-type and *Ccp1*<sup>-/-</sup> conditions from the same experiments.

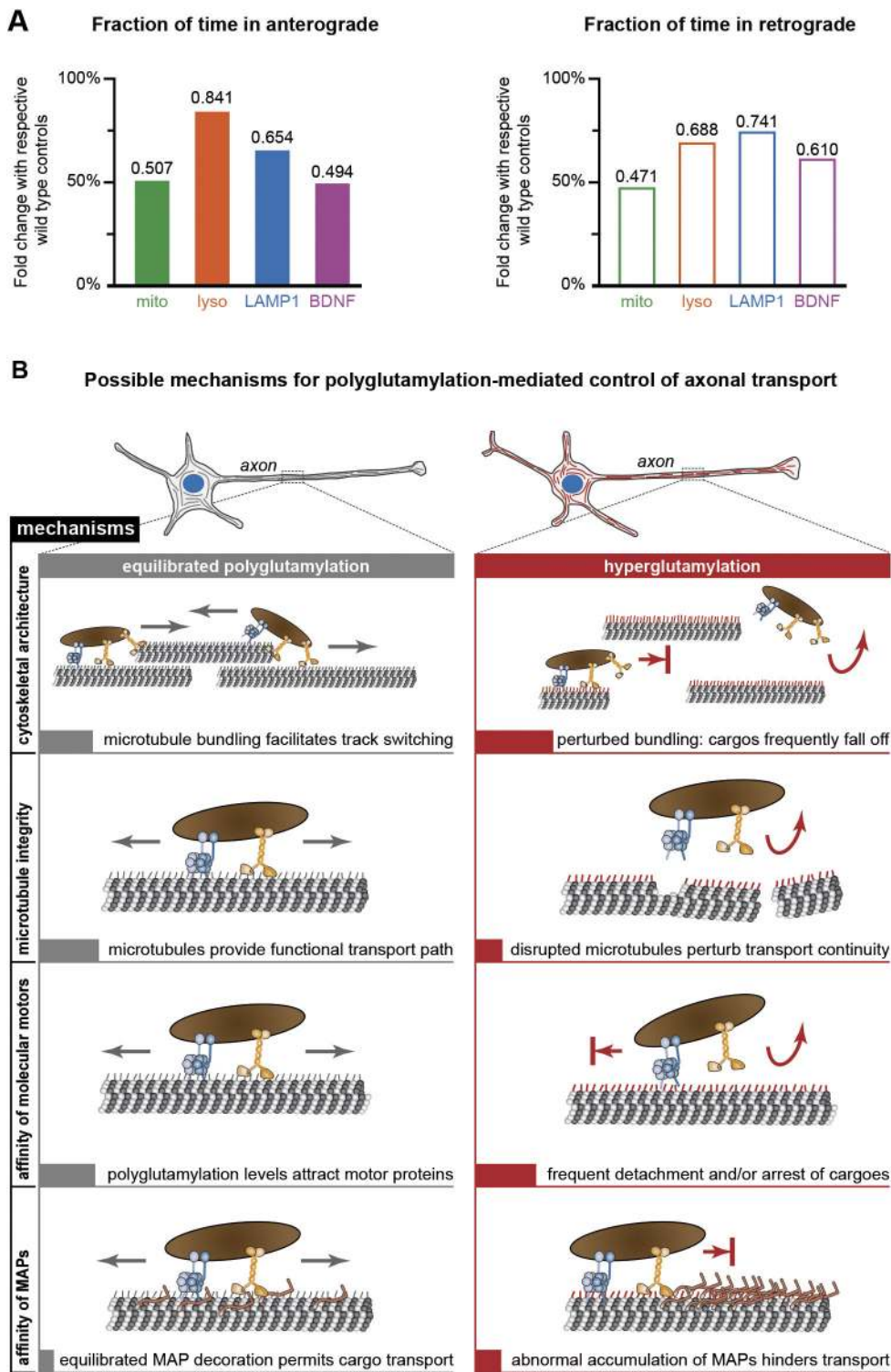


**Fig. 7. Tubulin hyperglutamylation reduces the overall motility of all cargoes analysed.** (A) Bar graphs representing the relative amount of time different vesicles spent in anterograde (filled bars) and retrograde (open bars) movement in *Ccp1*<sup>-/-</sup> neurons. Mitochondria and BDNF vesicles show the strongest decrease of motility in *Ccp1*<sup>-/-</sup> neurons. (B) Schematic representation of possible mechanisms by which tubulin polyglutamylation could regulate axonal transport, and the predicted impacts of hyperglutamylation. Excessive levels of polyglutamylation (red tails on the microtubules) could affect the switching of cargoes between microtubule tracks, which is a rate-limiting factor for efficient transport (Yogev et al., 2016). Hyperglutamylation could also cause frequent detachment of cargoes from the microtubule tracks, either indirectly by disrupting microtubules (Lacroix et al., 2010; Valenstein and Roll-Mecak, 2016) and by abnormal accumulation of MAPs (Vershinin et al., 2007) that could act as 'roadblocks', or directly by modulating the affinity of motor proteins to the microtubule tracks (Sirajuddin et al., 2014).

[polyE, 1:10,000 (vol/vol); AdipoGen, AG-25B-0030] to determine differences in tubulin modifications at equal tubulin levels. Chemiluminescence signal on the membrane was revealed using Clarity Western ECL Substrate (Bio-Rad, 1705060) solution.

#### Mouse hippocampal neuron cultures

Hippocampal neuron cultures were performed according to standard protocols described earlier (Bodakuntla et al., 2020a; Kaech and Banker, 2006). Briefly, pregnant mice at 17.5 days of gestation were sacrificed using cervical dislocation, the embryos were decapitated and hippocampi of

individual embryos were collected in separate tubes. At the same time, a piece of brain tissue from the individual embryos was collected, subjected to lysis using REDExtract-N-Amp Tissue PCR Kit (Sigma, XNAT) and analysed for the *Ccp1* gene. Collected hippocampi were enzymatically and mechanically dissociated using trypsin and fire-polished Pasteur pipettes, respectively. Based on the genotyping results, only wild-type and *Ccp1*<sup>-/-</sup> hippocampal neurons were counted and plated on poly-D-lysine (354210, Corning)-coated plastic dishes for immunoblot analysis or on glass-bottom dishes (81158, Ibidi) for live-cell imaging (transport analysis). A schematic representation of the work flow is given in Fig. 1C.



### Cloning and DNA plasmids

Cre-recombinase and vesicle markers (LAMP1) were cloned in to pTRIP lentiviral vectors using sequence- and ligation-independent cloning (Jeong et al., 2012), which was described in detail in our earlier studies (Bodakuntla et al., 2020a). Briefly, cre-recombinase was amplified using primers with at least 15 bp of homology sequence to the ends of the target vector and inserted in the pTRIP vector with CMV-enhanced chicken  $\beta$ -actin (CAG) promoter at the XhoI site. The cre-recombinase was cloned after a self-cleavable 2A peptide sequence (Kim et al., 2011), which was in frame with the GFP. The *Lamp1* gene, a marker for late endosomes, was inserted at the NheI site, creating a C-terminally GFP-tagged protein. Primers used for amplification of cre-recombinase and *Lamp1* were: NLS-cre-FS-2A, 5'-tccactagtgtcgacATGCCCAAGAAGAAGAGGAAGGTG-3'; NLS-cre-FS-2A, 5'-catgtttttctaggtTAATCGCCATCTTCCAGCAGGC-3'; mLAMP1-FS1, 5'-agaattattccgctagcATGGCGGCCCGCCGCGCCCGCG-3'; and mLAMP1-RS1, 5'-accatGGTGGCgctagcGATGGTCTGATAGCCGGCGT-GACTCC-3'. Packaging plasmids pSPAX2 and pCMV-VSVG were Addgene plasmid #12260 (deposited by D. Trono) and Addgene plasmid #8454 (deposited by B. Weinberg), respectively. BDNF-mCherry was a kind gift from F. Saudou (Grenoble Institute of Neurosciences, France).

### Lentivirus production and transduction

Lentiviral particles were produced using protocols described earlier (Bodakuntla et al., 2020a). Briefly, X-Lenti 293T cells (Takara, 632180) plated in six-well plates were co-transfected with 1.6  $\mu$ g plasmid of interest and packaging plasmids (0.4  $\mu$ g of pCMV-VSVG and 1.6  $\mu$ g of pSPAX2) using 8  $\mu$ l of TransIT-293 (#MIR 2705, Mirus Bio) transfection reagent per well. On the next day, the culture medium was changed to Neurobasal medium (Thermo Fisher #21103049) supplemented with 1 $\times$  penicillin-streptomycin (Life Technologies, 15140130). Next day, the virus-containing supernatants were harvested, passed through a 0.45  $\mu$ m filter and either used fresh or aliquoted, and stored at  $-80^{\circ}\text{C}$ . To determine the optimal amount of virus for transduction, lentivirus aliquots were thawed, and different volumes were added to cultured primary neurons. Based on the expression levels of the GFP protein, the desired amount of virus to achieve maximum transduction efficiency was determined. On DIV0, *Ccp1*<sup>flx/flx</sup>*Ccp6*<sup>flx/flx</sup> hippocampal neurons were either left untransduced for controls or transduced with lentiviruses encoding GFP alone (control) or GFP-2A-cre-recombinase in order to transform the flox genes into knockouts. For transport experiments, wild-type and *Ccp1*<sup>-/-</sup> neurons were transduced with lentiviruses encoding either LAMP1-GFP or BDNF-mCherry.

### Imaging of axonal transport

Transport assays and analysis paradigms were designed based on established protocols (Ghiretti et al., 2016; Klinman and Holzbaun, 2016) and are described in detail earlier (Bodakuntla et al., 2020b). Briefly, for all transport experiments, neurons were imaged on DIV4. For imaging mitochondria or lysosome movements in the axon, neurons were incubated, respectively, with 2 nM MitoTracker Red CMXRos (Thermo Fisher, M7512) for 1 min or 100 nM LysoTracker Red DND-99 (Thermo Fisher, L7528) for 30 min in the cell culture incubator. After the staining, neurons were washed once with conditioned medium. Conditioned medium is neurobasal medium containing 1 $\times$  B27 (Thermo Fisher #17504044) and 1 $\times$  GlutaMax (Thermo Fisher #35050038) is taken from untreated DIV4 neurons.

For imaging LAMP1-GFP and BDNF-mCherry vesicles, DIV0 neurons were transduced with lentivirus encoding LAMP1-GFP and BDNF-mCherry, differentiated until DIV4 and washed once with conditioned medium before imaging. Particle movements were immediately imaged using a Nikon Ti-E spinning disk inverted confocal laser microscope equipped with a 60 $\times$  oil-immersion objective (N.A. 1.40). Images were captured using an ORCA-Flash 4.0 camera (Hamamatsu) set at 2 $\times$ 2 binning, and operated through Leica MM AF imaging software. All particle movements were recorded every 300 ms for 1 min in stream mode, with the imaging chamber set at 37 $^{\circ}\text{C}$  and 5%  $\text{CO}_2$ . For each experiment, at least five neurons per treatment group were imaged, without exceeding 30 min of imaging time per dish. A schematic representation of the work flow is given in Fig. 1C.

### Quantification of axonal transport

All the image processing and transport analysis procedures have been described in detail elsewhere (Bodakuntla et al., 2020b). All the data analyses were performed using ImageJ 1.47v with KymoToolBox plug-in (Zala et al., 2013) (available upon request from F. Cordelières, Bordeaux Imaging Center, France). Refer to [https://github.com/fabricecordelieres/IJ-Plugin\\_KymoToolBox](https://github.com/fabricecordelieres/IJ-Plugin_KymoToolBox) for a detailed explanation of the plug-in. For each movie, a maximum-intensity projection of the time lapse movie was generated, and the paths of particle movements along the longest neurite – the axon – were manually traced. The KymoToolBox plug-in was used to generate kymostacks (straightened videos of particle movements in the axons; Movies 1–4, lower panels) and kymographs calibrated in the  $x$ -axis (distance in  $\mu\text{m}$ ) and  $y$ -axis (time in seconds; Figs 2B, 3B, 4B and 5B). The kymographs were then analysed by manually tracing each distinct run of the trajectory of a particle using the segmented line tool from ImageJ. In our analyses, a 'run' was defined as the continuous movement of a given particle without changes in speed or direction. Runs with speeds lower than 0.10  $\mu\text{m/s}$ , or shorter than 0.9  $\mu\text{m}$  (corresponds to five pixels in our system and equivalent to the average size of the particles imaged) were not considered. To distinguish two consecutive runs in the same direction, we first traced a linear slope for the entire trajectory. If this linear trace did not follow the initial trajectory of the particle (minimum offset: three pixels, corresponding to  $\sim 0.5 \mu\text{m}$ ), we defined a novel run with a different trajectory. Although we are aware that some trajectories leave the imaging windows, we still included them in our analyses. Considering that our readouts are comparisons between wild-type and *Ccp1*<sup>-/-</sup> neurons, eventual biases introduced by this analysis paradigm will equally be present in both conditions, and thus will not significantly influence the final results. The plug-in generates a kymograph, highlighting the anterograde runs in green, retrograde runs in red and immotile trajectories in blue (kymographs of one experiment are shown in Figs 2B, 3B, 4B and 5B). A schematic representation of the work flow is given in Fig. 1C.

The run length and run time transport parameters were measured as shown in Fig. 1C, and run speed and overall motility were calculated (Figs S2, S3, S4 and S5). For each experiment, run length and run speed distributions from each condition were plotted and medians of the distributions were compared. Overall motility, the percentage of time that particles spend in movement in the given observation time is calculated for each condition. A motility of 100% means that all detected particles in the kymograph were in movement for the whole duration of observation time (60 s).

Overall motility [%] =

$$\frac{\text{Sum of all run times in kymograph} : \sum T_1 \dots T_n [\text{s}]}{\text{Number of particles in kymograph} \times \text{Imaging time} [\text{s}]} \times 100$$

Particle density is calculated as the number of particles per length of the axon. The 'average run length' (Figs 2G, 3G, 4G and 5G) and 'average run speed' (Fig. 2H, 3H, 4H and 5H) were determined by calculating the mean of all medians (Figs S2, S3, S4 and S5). The 'average overall motility' (Figs 2I, 3I, 4I and 5I) and 'average vesicle density' (Figs 2J, 3J, 4J and 5J) were determined by calculating the mean of the respective values from all the experiments (Figs S2, S3, S4 and S5). Bin analyses were performed to determine the probability of long vesicle runs. Bin widths were set at approximately twice the median values: 3  $\mu\text{m}$  for anterograde runs of mitochondria and lysosomes; 6  $\mu\text{m}$  for anterograde runs of LAMP1-GFP and BDNF-mCherry vesicles; 5  $\mu\text{m}$  for all retrograde runs (Fig. 6).

### Statistical analyses

qPCR analysis for tubulin-modifying enzymes was performed in samples collected from three independent experiments. The analyses for all the samples in an experiment were performed simultaneously in a single qPCR run. Data obtained from three independent experiments are shown as mean  $\pm$  s.d. (Fig. S1).

For statistical analyses of transport parameters, values for run length and speed of a single experiment were represented as scatter plots with a line indicating a median and whiskers at interquartile ranges (25th and 75th percentiles; Figs S2A,B, S3A,B, S4A,B and S5A,B). Fraction of time spent

in movement (overall motility) and particle density in the axon were calculated and are represented as bar graphs (Figs S2C,D, S3C,D, S4C,D and S5C,D). All experiments have been performed at least in triplicate. Medians of the run length and speed distributions from all the experiments were averaged, and are shown as mean±s.e.m. (Figs 2G,H, 3G,H, 4G,H and 5G,H). Overall motility and particle densities calculated in individual experiments were averaged and are shown as mean±s.e.m. (Figs 2I,J, 3I,J, 4I,J and 5I,J). The statistical significance of differences in particle densities was tested using a Mann–Whitney test and *P*-values are given. The statistical significance of differences in average run length, average speed and average overall motility was tested using a two-way ANOVA with a post-hoc by Bonferroni multiple comparison test and *P* values are given. The statistical significance of differences in qPCR analyses shown in Fig. S1 was tested using one-way ANOVA with a post-hoc by Bonferroni multiple comparison test and *P*-values are given. All the numerical values used for quantification of axonal transport are shown in Table S2.

#### Acknowledgements

We thank C. Alberti, E. Belloir, F. Bertrand, G. Buhagiar, C. Caspersen, V. Dangles-Marie, S. Gadadhar, I. Grandjean, H. Hermange, F. Maksut, C. Serieysson, M. Sittewelle, A. Thadal, A. Zeggai (Institut Curie) for technical assistance. We are grateful to M.-N. Soler, C. Lovo and L. Besse from the PICT-IBiSA at Orsay Imaging Facility of the Institut Curie supported by the Agence Nationale de la Recherche through the 'Investment for the future' program (France-Biome, ANR-10-INSB-04); to N. Manel (Institut Curie, Paris) for material and advice for the lentivirus production; and to F. Saudou for providing essential material. We also thank F. P. Cordelières (Bordeaux Imaging Center, France) for the KymoToolBox plug-in, as well as M. Brill (Technical University Munich, Germany), R. Chabrier, F. Del Bene and V. Marthiens (Institut Curie) for instructive discussions and advice.

#### Competing interests

The authors declare no competing or financial interests.

#### Author contributions

Conceptualization: S.B., C.J., M.M.M.; Methodology: S.B., A.S., C.V., C.G.-B., I.B., C.J., M.M.M.; Validation: S.B., A.S., I.B., C.J., M.M.M.; Formal analysis: S.B., A.S., C.V., I.B., C.J., M.M.M.; Investigation: S.B., A.S., C.J., M.M.M.; Writing - original draft: S.B., C.J., M.M.M.; Writing - review & editing: S.B., C.J., M.M.M.; Visualization: S.B., I.B., C.J., M.M.M.; Supervision: C.G.-B., I.B., C.J., M.M.M.; Project administration: C.J., M.M.M.; Funding acquisition: S.B., C.G.-B., C.J., M.M.M.

#### Funding

This work was supported by the Agence Nationale de la Recherche (ANR-10-IDEX-0001-02) and by LabEx CellTisPhyBio (ANR-11-LBX-0038). C.J. is supported by the Institut Curie, the Agence Nationale de la Recherche (ANR-12-BSV2-0007 and ANR-17-CE13-0021), the Institut National Du Cancer (2014-PL BIO-11-ICR-1) and the Fondation pour la Recherche Medicale (DEQ20170336756). M.M.M. is supported by an European Molecular Biology Organization short-term fellowship (ASTF 148-2015) and by the Fondation Vaincre Alzheimer (FR-16055p), and S.B. is supported by the Fondation pour la Recherche Medicale (FDT201805005465). S.B., C.V., C.G.-B. and C.J. are supported by the Evaluación y Orientación de la Cooperación Científica - Comisión Nacional de Investigación Científica y Tecnológica (C14B01).

#### Supplementary information

Supplementary information available online at <http://jcs.biologists.org/lookup/doi/10.1242/jcs.241802.supplemental>

#### Peer review history

The peer review history is available online at <https://jcs.biologists.org/lookup/doi/10.1242/jcs.241802.reviewer-comments.pdf>

#### References

Alexander, J. E., Hunt, D. F., Lee, M. K., Shabanowitz, J., Michel, H., Berlin, S. C., MacDonald, T. L., Sundberg, R. J., Rebhun, L. I. and Frankfurter, A. (1991). Characterization of posttranslational modifications in neuron-specific class III beta-tubulin by mass spectrometry. *Proc. Natl. Acad. Sci. USA* **88**, 4685-4689. doi:10.1073/pnas.88.11.4685

Ashrafi, G., Schlehe, J. S., LaVoie, M. J. and Schwarz, T. L. (2014). Mitophagy of damaged mitochondria occurs locally in distal neuronal axons and requires PINK1 and Parkin. *J. Cell Biol.* **206**, 655-670. doi:10.1083/jcb.201401070

Barisic, M., Silva e Sousa, R., Tripathy, S. K., Magiera, M. M., Zaytsev, A. V., Pereira, A. L., Janke, C., Grishchuk, E. L. and Maiato, H. (2015). Microtubule

detyrosination guides chromosomes during mitosis. *Science* **348**, 799-803. doi:10.1126/science.aaa5175

Bentley, M. and Banker, G. (2016). The cellular mechanisms that maintain neuronal polarity. *Nat. Rev. Neurosci.* **17**, 611-622. doi:10.1038/nrn.2016.100

Bièche, I., Onody, P., Laurendeau, I., Olivi, M., Vidaud, D., Lidereau, R. and Vidaud, M. (1999). Real-time reverse transcription-PCR assay for future management of ERBB2-based clinical applications. *Clin. Chem.* **45**, 1148-1156.

Bodakuntla, S., Jijumon, A. S., Villablanca, C., Gonzalez-Billault, C. and Janke, C. (2019). Microtubule-associated proteins: structuring the cytoskeleton. *Trends Cell Biol.* **29**, 804-819. doi:10.1016/j.tcb.2019.07.004

Bodakuntla, S., Janke, C. and Magiera, M. M. (2020a). Knocking out multiple genes in cultured primary neurons to study tubulin posttranslational modifications. *Cytoskeleton Dynamics - Methods and Protocols*, vol. 2101 (ed. H. Maiato), pp. 327-351. New York: Springer US.

Bodakuntla, S., Magiera, M. M. and Janke, C. (2020b). Determining the role of tubulin posttranslational modifications on axonal transport. *Cytoskeleton Dynamics - Methods and Protocols*, vol. 2101 (ed. H. Maiato), pp. 353-370. New York: Springer US.

Bonnet, C., Boucher, D., Lazereg, S., Pedrotti, B., Islam, K., Denoulet, P. and Larcher, J. C. (2001). Differential binding regulation of microtubule-associated proteins MAP1A, MAP1B, and MAP2 by tubulin polyglutamylation. *J. Biol. Chem.* **276**, 12839-12848. doi:10.1074/jbc.M011380200

Boucher, D., Larcher, J.-C., Gros, F. and Denoulet, P. (1994). Polyglutamylation of tubulin as a progressive regulator of in vitro interactions between the microtubule-associated protein Tau and tubulin. *Biochemistry* **33**, 12471-12477. doi:10.1021/bi00207a014

Brady, S. T. and Morfini, G. A. (2017). Regulation of motor proteins, axonal transport deficits and adult-onset neurodegenerative diseases. *Neurobiol. Dis.* **105**, 273-282. doi:10.1016/j.nbd.2017.04.010

Cavanagh, J. B. (1984). The problems of neurons with long axons. *Lancet* **1**, 1284-1287. doi:10.1016/S0140-6736(84)92457-7

Chen, J., Kanai, Y., Cowan, N. J. and Hirokawa, N. (1992). Projection domains of MAP2 and tau determine spacings between microtubules in dendrites and axons. *Nature* **360**, 674-677. doi:10.1038/360674a0

Cheng, X.-T., Xie, Y.-X., Zhou, B., Huang, N., Farfel-Becker, T. and Sheng, Z.-H. (2018). Characterization of LAMP1-labeled nondegradative lysosomal and endocytic compartments in neurons. *J. Cell Biol.* **217**, 3127-3139. doi:10.1083/jcb.201711083

Choquet, D. and Triller, A. (2013). The dynamic synapse. *Neuron* **80**, 691-703. doi:10.1016/j.neuron.2013.10.013

Conde, C. and Cáceres, A. (2009). Microtubule assembly, organization and dynamics in axons and dendrites. *Nat. Rev. Neurosci.* **10**, 319-332. doi:10.1038/nrn2631

DeFelipe, J. (2013). Cajal and the discovery of a new artistic world: the neuronal forest. *Prog. Brain Res.* **203**, 201-220. doi:10.1016/B978-0-444-62730-8.00008-6

Dompierre, J. P., Godin, J. D., Charrin, B. C., Cordelières, F. P., King, S. J., Humbert, S. and Saudou, F. (2007). Histone deacetylase 6 inhibition compensates for the transport deficit in Huntington's disease by increasing tubulin acetylation. *J. Neurosci.* **27**, 3571-3583. doi:10.1523/JNEUROSCI.0037-07.2007

Eddé, B., Rossier, J., Le Caer, J. P., Desbryères, E., Gros, F. and Denoulet, P. (1990). Posttranslational glutamylation of alpha-tubulin. *Science* **247**, 83-85. doi:10.1126/science.1967194

Ghiretti, A. E., Thies, E., Tokito, M. K., Lin, T., Ostap, E. M., Kneussel, M. and Holzbaur, E. L. F. (2016). Activity-dependent regulation of distinct transport and cytoskeletal remodeling functions of the dendritic kinesin KIF21B. *Neuron* **92**, 857-872. doi:10.1016/j.neuron.2016.10.003

Gilmore-Hall, S., Kuo, J., Ward, J. M., Zahra, R., Morrison, R. S., Perkins, G. and La Spada, A. R. (2019). CCP1 promotes mitochondrial fusion and motility to prevent Purkinje cell neuron loss in pcd mice. *J. Cell Biol.* **218**, 206-219. doi:10.1083/jcb.201709028

Guedes-Dias, P. and Holzbaur, E. L. F. (2019). Axonal transport: driving synaptic function. *Science* **366**, eaaw9997. doi:10.1126/science.aaw9997

Harada, A., Oguchi, K., Okabe, S., Kuno, J., Terada, S., Ohshima, T., Sato-Yoshitake, R., Takei, Y., Noda, T. and Hirokawa, N. (1994). Altered microtubule organization in small-calibre axons of mice lacking tau protein. *Nature* **369**, 488-491. doi:10.1038/369488a0

Her, L.-S. and Goldstein, L. S. B. (2008). Enhanced sensitivity of striatal neurons to axonal transport defects induced by mutant huntingtin. *J. Neurosci.* **28**, 13662-13672. doi:10.1523/JNEUROSCI.4144-08.2008

Hirokawa, N., Niwa, S. and Tanaka, Y. (2010). Molecular motors in neurons: transport mechanisms and roles in brain function, development, and disease. *Neuron* **68**, 610-638. doi:10.1016/j.neuron.2010.09.039

Ikegami, K., Mukai, M., Tsuchida, J.-I., Heier, R. L., Macgregor, G. R. and Setou, M. (2006). TTL7 is a mammalian beta-tubulin polyglutamylation required for growth of MAP2-positive neurites. *J. Biol. Chem.* **281**, 30707-30716. doi:10.1074/jbc.M603984200

Ikegami, K., Heier, R. L., Taruishi, M., Takagi, H., Mukai, M., Shimma, S., Taira, S., Hatanaka, K., Morone, N., Yao, I. et al. (2007). Loss of alpha-tubulin polyglutamylation in ROSA22 mice is associated with abnormal targeting of



- KIF1A and modulated synaptic function. *Proc. Natl. Acad. Sci. USA* **104**, 3213–3218. doi:10.1073/pnas.0611547104
- Janke, C. (2014). The tubulin code: molecular components, readout mechanisms, and functions. *J. Cell Biol.* **206**, 461–472. doi:10.1083/jcb.201406055
- Janke, C., Rogowski, K., Wloga, D., Regnard, C., Kajava, A. V., Strub, J.-M., Temurak, N., van Dijk, J., Boucher, D., van Dorsseleer, A. et al. (2005). Tubulin polyglutamylase enzymes are members of the TTL domain protein family. *Science* **308**, 1758–1762. doi:10.1126/science.1113010
- Jeong, J.-Y., Yim, H.-S., Ryu, J.-Y., Lee, H. S., Lee, J.-H., Seen, D.-S. and Kang, S. G. (2012). One-step sequence- and ligation-independent cloning as a rapid and versatile cloning method for functional genomics studies. *Appl. Environ. Microbiol.* **78**, 5440–5443. doi:10.1128/AEM.00844-12
- Kaech, S. and Banker, G. (2006). Culturing hippocampal neurons. *Nat. Protoc.* **1**, 2406–2415. doi:10.1038/nprot.2006.356
- Kalinina, E., Biswas, R., Berezniuk, I., Hermoso, A., Aviles, F. X. and Fricker, L. D. (2007). A novel subfamily of mouse cytosolic carboxypeptidases. *FASEB J.* **21**, 836–850. doi:10.1096/fj.06-7329.com
- Karakaya, M., Paketci, C., Altmueller, J., Thiele, H., Hoelker, I., Yis, U. and Wirth, B. (2019). Biallelic variant in AGTPBP1 causes infantile lower motor neuron degeneration and cerebellar atrophy. *Am. J. Med. Genet. A* **179**, 1580–1584. doi:10.1002/ajmg.a.61198
- Kim, J. H., Lee, S.-R., Li, L.-H., Park, H.-J., Park, J.-H., Lee, K. Y., Kim, M.-K., Shin, B. A. and Choi, S.-Y. (2011). High cleavage efficiency of a 2A peptide derived from porcine teschovirus-1 in human cell lines, zebrafish and mice. *PLoS ONE* **6**, e18556. doi:10.1371/journal.pone.0018556
- Kim, J.-Y., Woo, S.-Y., Hong, Y. B., Choi, H., Kim, J., Choi, H., Mook-Jung, I., Ha, N., Kyung, J., Koo, S. K. et al. (2016). HDAC6 inhibitors rescued the defective axonal mitochondrial movement in motor neurons derived from the induced pluripotent stem cells of peripheral neuropathy patients with HSPB1 mutation. *Stem Cells Int.* **2016**, 9475981. doi:10.1155/2016/9475981
- Klinman, E. and Holzbaur, E. L. F. (2016). Comparative analysis of axonal transport markers in primary mammalian neurons. *Methods Cell Biol.* **131**, 409–424. doi:10.1016/bs.mcb.2015.06.011
- Konishi, Y. and Setou, M. (2009). Tubulin tyrosination navigates the kinesin-1 motor domain to axons. *Nat. Neurosci.* **12**, 559–567. doi:10.1038/nn.2314
- Lacroix, B., van Dijk, J., Gold, N. D., Guizetti, J., Aldrian-Herrada, G., Rogowski, K., Gerlich, D. W. and Janke, C. (2010). Tubulin polyglutamylation stimulates spastin-mediated microtubule severing. *J. Cell Biol.* **189**, 945–954. doi:10.1083/jcb.201001024
- Lee, C. W. and Peng, H. B. (2008). The function of mitochondria in presynaptic development at the neuromuscular junction. *Mol. Biol. Cell* **19**, 150–158. doi:10.1091/mbc.e07-05-0515
- Lee, S., Sato, Y. and Nixon, R. A. (2011). Lysosomal proteolysis inhibition selectively disrupts axonal transport of degradative organelles and causes an Alzheimer's-like axonal dystrophy. *J. Neurosci.* **31**, 7817–7830. doi:10.1523/JNEUROSCI.6412-10.2011
- Lessard, D. V., Zinder, O. J., Hotta, T., Verhey, K. J., Ohi, R. and Berger, C. L. (2019). Polyglutamylation of tubulin's C-terminal tail controls pausing and motility of kinesin-3 family member KIF1A. *J. Biol. Chem.* **294**, 6353–6363. doi:10.1074/jbc.RA118.005765
- Lo, K. Y., Kuzmin, A., Unger, S. M., Petersen, J. D. and Silverman, M. A. (2011). KIF1A is the primary anterograde motor protein required for the axonal transport of dense-core vesicles in cultured hippocampal neurons. *Neurosci. Lett.* **491**, 168–173. doi:10.1016/j.neulet.2011.01.018
- Lu, B., Nagappan, G., Guan, X., Nathan, P. J. and Wren, P. (2013). BDNF-based synaptic repair as a disease-modifying strategy for neurodegenerative diseases. *Nat. Rev. Neurosci.* **14**, 401–416. doi:10.1038/nrn3505
- Maas, C., Belgardt, D., Lee, H. K., Heisler, F. F., Lappe-Siefke, C., Magiera, M. M., van Dijk, J., Hausrat, T. J., Janke, C. and Kneussel, M. (2009). Synaptic activation modifies microtubules underlying transport of postsynaptic cargo. *Proc. Natl. Acad. Sci. USA* **106**, 8731–8736. doi:10.1073/pnas.0812391106
- Maday, S., Wallace, K. E. and Holzbaur, E. L. F. (2012). Autophagosomes initiate distally and mature during transport toward the cell soma in primary neurons. *J. Cell Biol.* **196**, 407–417. doi:10.1083/jcb.201106120
- Maday, S., Twelvetrees, A. E., Moughamian, A. J. and Holzbaur, E. L. F. (2014). Axonal transport: cargo-specific mechanisms of motility and regulation. *Neuron* **84**, 292–309. doi:10.1016/j.neuron.2014.10.019
- Magiera, M. M., Bodakuntla, S., Žiak, J., Lacomme, S., Marques Sousa, P., Leboucher, S., Hausrat, T. J., Bosc, C., Andrieux, A., Kneussel, M. et al. (2018). Excessive tubulin polyglutamylation causes neurodegeneration and perturbs neuronal transport. *EMBO J.* **37**, e100440. doi:10.15252/emboj.2018100440
- Millecamps, S. and Julien, J.-P. (2013). Axonal transport deficits and neurodegenerative diseases. *Nat. Rev. Neurosci.* **14**, 161–176. doi:10.1038/nrn3380
- Morris, R. L. and Hollenbeck, P. J. (1993). The regulation of bidirectional mitochondrial transport is coordinated with axonal outgrowth. *J. Cell Sci.* **104**, 917–927.
- Moutaux, E., Christaller, W., Scaramuzzino, C., Genoux, A., Charlot, B., Cazorla, M. and Saudou, F. (2018). Neuronal network maturation differently affects secretory vesicles and mitochondria transport in axons. *Sci. Rep.* **8**, 13429. doi:10.1038/s41598-018-31759-x
- Muñoz-Castañeda, R., Díaz, D., Peris, L., Andrieux, A., Bosc, C., Muñoz-Castañeda, J. M., Janke, C., Alonso, J. R., Moutin, M.-J. and Weruaga, E. (2018). Cytoskeleton stability is essential for the integrity of the cerebellum and its motor- and affective-related behaviors. *Sci. Rep.* **8**, 3072. doi:10.1038/s41598-018-21470-2
- Newton, C. N., DeLuca, J. G., Himes, R. H., Miller, H. P., Jordan, M. A. and Wilson, L. (2002). Intrinsically slow dynamic instability of HeLa cell microtubules in vitro. *J. Biol. Chem.* **277**, 42456–42462. doi:10.1074/jbc.M207134200
- Nirschl, J. J., Ghirelli, A. E. and Holzbaur, E. L. F. (2017). The impact of cytoskeletal organization on the local regulation of neuronal transport. *Nat. Rev. Neurosci.* **18**, 585–597. doi:10.1038/nrn.2017.100
- Pu, J., Guardia, C. M., Keren-Kaplan, T. and Bonifacino, J. S. (2016). Mechanisms and functions of lysosome positioning. *J. Cell Sci.* **129**, 4329–4339. doi:10.1242/jcs.196287
- Reck-Peterson, S. L., Redwine, W. B., Vale, R. D. and Carter, A. P. (2018). The cytoplasmic dynein transport machinery and its many cargoes. *Nat. Rev. Mol. Cell Biol.* **19**, 382–398. doi:10.1038/s41580-018-0004-3
- Rogowski, K., van Dijk, J., Magiera, M. M., Bosc, C., Deloulme, J.-C., Bosson, A., Peris, L., Gold, N. D., Lacroix, B., Bosch Grau, M. et al. (2010). A family of protein-deglutamylation enzymes associated with neurodegeneration. *Cell* **143**, 564–578. doi:10.1016/j.cell.2010.10.014
- Rowland, K. C., Irby, N. K. and Spiro, G. A. (2000). Specialized synapse-associated structures within the calyx of Held. *J. Neurosci.* **20**, 9135–9144. doi:10.1523/JNEUROSCI.20-24-09135.2000
- Rüdiger, M., Plessman, U., Klöppel, K.-D., Wehland, J. and Weber, K. (1992). Class II tubulin, the major brain beta tubulin isotype is polyglutamylated on glutamic acid residue 435. *FEBS Lett.* **308**, 101–105. doi:10.1016/0014-5793(92)81061-P
- Shahpasand, K., Uemura, I., Saito, T., Asano, T., Hata, K., Shibata, K., Toyoshima, Y., Hasegawa, M. and Hisanaga, S.-I. (2012). Regulation of mitochondrial transport and inter-microtubule spacing by tau phosphorylation at the sites hyperphosphorylated in Alzheimer's disease. *J. Neurosci.* **32**, 2430–2441. doi:10.1523/JNEUROSCI.5927-11.2012
- Shashi, V., Magiera, M. M., Klein, D., Zaki, M., Schoch, K., Rudnik-Schöneborn, S., Norman, A., Lopes Abath Neto, O., Dusi, M., Yuan, X. et al. (2018). Loss of tubulin deglutamylation CCP1 causes infantile-onset neurodegeneration. *EMBO J.* **37**, e100540. doi:10.15252/emboj.2018100540
- Sheffer, R., Gur, M., Brooks, R., Salah, S., Daana, M., Fraenkel, N., Eisenstein, E., Rabie, M., Nevo, Y., Jalas, C. et al. (2019). Biallelic variants in AGTPBP1, involved in tubulin deglutamylation, are associated with cerebellar degeneration and motor neuropathy. *Eur. J. Hum. Genet.* **27**, 1419–1426. doi:10.1038/s41431-019-0400-y
- Sirajuddin, M., Rice, L. M. and Vale, R. D. (2014). Regulation of microtubule motors by tubulin isotypes and post-translational modifications. *Nat. Cell Biol.* **16**, 335–344. doi:10.1038/ncb2920
- Sleigh, J. N., Rossor, A. M., Fellows, A. D., Tosolini, A. P. and Schiavo, G. (2019). Axonal transport and neurological disease. *Nat. Rev. Neurol.* **15**, 691–703. doi:10.1038/s41582-019-0257-2
- Stephan, R., Goellner, B., Moreno, E., Frank, C. A., Hugenschmidt, T., Genoud, C., Aberle, H. and Pielage, J. (2015). Hierarchical microtubule organization controls axon caliber and transport and determines synaptic structure and stability. *Dev. Cell* **33**, 5–21. doi:10.1016/j.devcel.2015.02.003
- Tas, R. P., Chazeau, A., Cloin, B. M. C., Lambers, M. L. A., Hoogenraad, C. C. and Kapitein, L. C. (2017). Differentiation between oppositely oriented microtubules controls polarized neuronal transport. *Neuron* **96**, 1264–1271.e5. doi:10.1016/j.neuron.2017.11.018
- Tort, O., Tanco, S., Rocha, C., Bièche, I., Seixas, C., Bosc, C., Andrieux, A., Moutin, M.-J., Xavier Avilés, F., Lorenzo, J. et al. (2014). The cytosolic carboxypeptidases CCP2 and CCP3 catalyze posttranslational removal of acidic amino acids. *Mol. Biol. Cell* **25**, 3017–3027. doi:10.1091/mbc.e14-06-1072
- Tortosa, E., Kapitein, L. C. and Hoogenraad, C. C. (2016). Microtubule organization and microtubule-associated proteins (MAPs). In *Dendrites: Development and Disease* (ed. K. Emoto, R. Wong, E. Huang and C. Hoogenraad), pp. 31–75. Springer Japan.
- Valenstein, M. L. and Roll-Mecak, A. (2016). Graded control of microtubule severing by tubulin glutamylation. *Cell* **164**, 911–921. doi:10.1016/j.cell.2016.01.019
- van Dijk, J., Rogowski, K., Miro, J., Lacroix, B., Eddé, B. and Janke, C. (2007). A targeted multienzyme mechanism for selective microtubule polyglutamylation. *Mol. Cell* **26**, 437–448. doi:10.1016/j.molcel.2007.04.012
- Vélez, J. I., Lopera, F., Patel, H. R., Johar, A. S., Cai, Y., Rivera, D., Tobón, C., Villegas, A., Sepulveda-Falla, D., Lehmann, S. G. et al. (2016). Mutations modifying sporadic Alzheimer's disease age of onset. *Am. J. Med. Genet. B Neuropsychiatr. Genet.* **171**, 1116–1130. doi:10.1002/ajmg.b.32493
- Vershinin, M., Carter, B. C., Razafsky, D. S., King, S. J. and Gross, S. P. (2007). Multiple-motor based transport and its regulation by Tau. *Proc. Natl. Acad. Sci. USA* **104**, 87–92. doi:10.1073/pnas.0607919104
- Virlogeux, A., Moutaux, E., Christaller, W., Genoux, A., Bruyère, J., Fino, E., Charlot, B., Cazorla, M. and Saudou, F. (2018). Reconstituting corticostriatal



- network on-a-chip reveals the contribution of the presynaptic compartment to Huntington's disease. *Cell Rep.* **22**, 110-122. doi:10.1016/j.celrep.2017.12.013
- Yogev, S., Cooper, R., Fetter, R., Horowitz, M. and Shen, K.** (2016). Microtubule organization determines axonal transport dynamics. *Neuron* **92**, 449-460. doi:10.1016/j.neuron.2016.09.036
- Zala, D., Hinckelmann, M.-V., Yu, H., Lyra da Cunha, M. M., Liot, G., Cordelières, F. P., Marco, S. and Saudou, F.** (2013). Vesicular glycolysis provides on-board energy for fast axonal transport. *Cell* **152**, 479-491. doi:10.1016/j.cell.2012.12.029
- Zeng, H. and Sanes, J. R.** (2017). Neuronal cell-type classification: challenges, opportunities and the path forward. *Nat. Rev. Neurosci.* **18**, 530-546. doi:10.1038/nrn.2017.85
- Zhou, B., Yu, P., Lin, M.-Y., Sun, T., Chen, Y. and Sheng, Z.-H.** (2016). Facilitation of axon regeneration by enhancing mitochondrial transport and rescuing energy deficits. *J. Cell Biol.* **214**, 103-119. doi:10.1083/jcb.201605101